Made available through Montana State University's ScholarWorks

Electrically tunable magnetic fluctuations in multilayered vanadium-doped tungsten diselenide

Lan-Anh T. Nguyen, Jinbao Jiang, Tuan Dung Nguyen, Philip Kim, Min-Kyu Joo, Dinh Loc Duong, Young Hee Lee

This version of the article has been accepted for publication, after peer review (when applicable) and is subject to Springer Nature's AM terms of use, but is not the Version of Record and does not reflect post-acceptance improvements, or any corrections. The Version of Record is available online at: http://dx.doi.org/10.1038/s41928-023-01002-1

Electrically tunable magnetic fluctuations in multilayered vanadium-doped tungsten diselenide

Lan-Anh T. Nguyen[1,2], Jinbao Jiang[3,4], Tuan Dung Nguyen[1,2], Philip Kim[5], Min-Kyu Joo[6,7]*, Dinh Loc Duong[1,2,8,9]*, Young Hee Lee[1,2,10]*

[1]Center for Integrated Nanostructure Physics (CINAP), Institute for Basic Science (IBS), Suwon 16419, Republic of Korea.

[2]Department of Energy Science, Sungkyunkwan University, Suwon 16419, Republic of Korea.

[3]College of Advanced Interdisciplinary Studies, National University of Defense Technology, Changsha 410073, China.

[4]Hunan Provincial Key Laboratory of Novel Nano-Optoelectronic Information Materials and Devices, National University of Defense Technology, Changsha 410073, China.

[5]John A. Paulson School of Engineering and Applied Sciences, Harvard University, Cambridge, Massachusetts 02138, USA.

[6]Department of Applied Physics, Sookmyung Women's University, Seoul 04310, Republic of Korea.

[7]Institute of Advanced Materials and Systems, Sookmyung Women's University, Seoul 04310, Republic of Korea.

[8]Department of Physics, Montana State University, Bozeman, MT 59717, United States.

[9] MonArk NSF Quantum Foundry, Montana State University, Bozeman, MT 59717, United States.

[10]Department of Physics, Sungkyunkwan University, Suwon 16419, Republic of Korea.

*email: mkjoo@sookmyung.ac.kr, l.duong1902@gmail.com, leeyoung@skku.edu

Fluctuations are ubiquitous in magnetic materials and can cause random telegraph noise. Such noise is of potential use in systems such as spiking neuron devices, random number generators, and probability bits. Here we report electrically tunable magnetic fluctuations and random telegraph noise in multilayered vanadium-doped tungsten diselenide (WSe_2). We use vertical tunneling heterostructure devices composed of graphene/vanadium-doped-WSe_2/graphene and magnetoresistance measurements. We identify bistable magnetic states through discrete Gaussian peaks in the random telegraph noise histogram and the $1/f^2$ features of the noise power spectrum. Three categories of fluctuations are detected: small resistance fluctuations at high temperatures due to intralayer coupling between magnetic domains; large resistance changes over a wide range of temperatures; and persistent large resistance changes at low temperatures due to magnetic interlayer coupling. We also show that the bistable state and the cut-off frequency of the random telegraph noise can be modulated with an electric field.

Random telegraph noise (RTN) in semiconductor devices is typically caused by two-state defects and can be used as a diagnosis and prediction tool to investigate device reliability[1,2]. The spike-like nature of RTN, which is similar to the stochastic activity of neuronal circuits in the brain, is also of use in applications such as random number generator, neuromorphic computing, and neural networks[3,4]. Furthermore, recent work has shown that the RTN in devices such as thermally unstable magnetic tunnelling junctions can be controlled and could be used as probability bits for computing[5–9].

RTN has also been observed in numerous quantum states[10–12], particularly at the critical transition point of magnetic materials[13,14]. At the transition point, these magnetic fluctuations become most readily apparent and can be detected with various techniques[15] including electrical measurements, where RTN generates resistance variances with an amplitude of around 0.1%[13]. Magnetic fluctuations should be inherently stronger and easier to control through external forces in two-dimensional (2D) magnetic materials than in their three-dimensional (3D) counterparts [16–18]. In the 2D van der Waals (vdW) material chromium tribromide ($CrBr_3$), magnetic fluctuations have been measured using the magneto-optic Kerr effect[17]. These fluctuations though appear over a narrow range of transition temperatures centered around 22 K and have not been measured via electrical means.

In this Article, we report magnetic fluctuations and RTN in a layered vdW semiconductor with a magnetic dopant: vanadium-doped tungsten diselenide (V-WSe2)[19]. We use vertical tunnel junctions composed of graphene/V-WSe_2/graphene, and resistance measurements across the devices show high-amplitude RTN of up to 40% between well-defined bistable states. Discrete Gaussian peaks in the RTN histogram and $1/f_2$ features in the noise power spectrum confirm the

bistable magnetic states in our system. The amplitude and RTN cut-off frequency can be tuned using magnetic fields, electric fields, and temperature.

Magnetoresistance characterisation

Our vertical heterostructure consisting of multilayered V-doped WSe_2 (0.1% V) sandwiched between two graphene layers (**Fig. 1a**). **Figure 1b** shows typical resistance changes with temperature of the device after zero-field cooling (ZFC) and field cooling (FC) at 1 T. In the high temperature region (region I), the resistance increases as the temperature decreases, typical of semiconductors. Below a temperature 140 K (region II), the resistance rapidly drops and large fluctuations are observed. The resistance increases again at temperatures below 70 K (region III). The resistance derivative shows that magnetic fluctuations persist over a wide range of temperatures. The largest fluctuations are observed in region II, which ranges from room temperature down to 2K, regardless of FC or ZFC condition. Magnetoresistance hysteresis and ferromagnetic order has been reported in V-doped WSe_2 multilayers as well as monolayers[19–21]. Interlayer magnetic coupling is considered to be weak at high temperatures and the magnetic order persists due to the intralayer coupling. The coexistence of intralayer and interlayer magnetic couplings may induce anomalous resistance changes and the giant fluctuations observed in our experiment.

We find the resistance fluctuation in our devices is dominated by two-state fluctuation, exhibiting RTN. **Figure 1c** shows the time evolution of resistance change for noise characteristics at 2 K. Characteristics of RTN are clearly visible under ZFC conditions, and manifest with two discrete states under FC conditions. The RTN amplitude is around ~5% after ZFC and is greatly enhanced to as large as ~30% after FC. Since there is no applied magnetic field during both RTN measurements, the sizable effect of RTN signals after FC (magnetic cooling with magnetic field)

indicates that the RTN originates from magnetic fluctuations in the V-doped WSe_2 layers rather than defects. These unexpectedly high noise amplitudes are in striking contrast with the amplitudes of < 0.1% seen in 3D magnetic materials such as lateral magnetic thin films (*e.g.*, GaMnAs and Cr)[13,22,23]. This giant RTN is correlated with the giant magnetoresistance (GMR) of vdW magnetic layers[24–27], which is likewise observed in a magnetic tunneling junction (MTJ) of CoFeB/MgO/CoFeB heterostructures[7].

In conventional MTJ for memory, the formation of two stable magnetic states (*e.g.*, antiparallel (AP) and parallel (P) states) between two magnetic layers produce low and high resistance states. The barrier of these two states is high enough to retain one stable state to persist for a long time. Meanwhile, the RTN appears when the switching barrier height between P and AP states is low in a stochastic MTJ by replacing the stable free magnetic layer by unstable or metastable magnetic layers (*e.g.*, reducing the thickness of magnetic layer)[7,8]. In our device, V-doped WSe_2 layers and van der Waals gaps are considered as magnetic layers and non-magnetic spacer, similar to MTJ[28–30], which plays a key role in producing large RTN, with a partial contribution from the reduced dimensionality[15,17]. This is analogous to the GMR observed in layered CrI_3 systems with a similar vertical device structure under a magnetic field[24–27]. Since the vanadium atoms are randomly distributed in the WSe_2 lattice, the observed giant RTN cannot be attributed to the presence of isolated aggregated magnetic dopants that happen in GaMnAs[23]. Such RTNs were consistently observed in a variety of V-doped WSe_2 devices (Supplementary Information Fig. 1), although the amplitudes differed slightly. WSe_2 layers without magnetic dopant showed low levels of random noises without distinctive RTN characteristics, and these were caused by intrinsic defects in the WSe_2 (Supplementary Information Fig. 2).

The RTN of magnetic fluctuation only appears for the unstable or metastable magnetic states (*e.g.*, superparamagnetic) to reduce the switching barrier height between P and AP couplings[7,8]. Therefore, the stable magnetic orders should be modified to transform to metastable/unstable magnetic orders. Although the V-doped WSe_2 monolayer with 0.1%V grown by chemical vapor deposition has demonstrated the Curie temperature (*T*c) at ~330 K with the strongest signal of magnetic domains at 0.3% V- doped WSe_2 from material point of view[19], we investigate magnetic properties of the MTJ devices at different V-doping concentrations by measuring the magnetoresistance.

Figure 2 shows out-of-plane and in-plane magnetoresistance (MR) of 0.1%, 0.3%, and 0.5% V-doped WSe_2 at 300 K with similar thicknesses of ~ 2 nm. We define MR(%)=[R(B)-R(0)]x100/R(0), out-of-plane MR hysteresis appears at 0.3% V and 0.5% V samples, clearly confirmed by ΔR (the resistance difference for forward (FW) and backward (BW) magnetic field, are defined as $\Delta R_{FW}(B) = [R_{FW}(B)-R_{BW}(-B)]/[R_{FW}(B)+R_{BW}(-B)]$ and $\Delta R_{BW}(B) = [R_{BW}(B)-R_{FW}(-B)]/ [R_{BW}(B)+R_{FW}(-B)]$, respectively), although such hysteresis is obscured at 0.1% V sample. The $R_{FW}(B)-R_{BW}(-B)$ should be zero in general for an ideal butterfly MR curve[31,32]. The ideal butterfly MR curve is symmetrical with +B and -B field in lateral device, which is usually observed with perpendicular ~~B~~ magnetic field. Nevertheless, this symmetrical butterfly MR (R_{xx}) curve is not always observed in some ferromagnetic semiconductors (*e.g.*, $Cr_2Ge_2Te_6$)[33]. In contrast to lateral device, our vertical device shows the additional asymmetric signal with B-field (*e.g.*, the resistance at negative B is different from that at positive B). Consequently, the asymmetrical MR hysteresis is manifested. The MR hysteresis is dominant up to 350 K at 0.3% V-doped WSe_2 with different bias (**Fig. 2b**), indicating that the Curie temperature is higher than 350 K, similar to

previous report[19]. In contrast, the MR hysteresis at 0.1% V is negligible and indicates the unstable or metastable magnetic order in 0.1% V-doped WSe_2, as evidenced by the strengthened RTN signals after FC. It explains the RTN appears solely in 0.1% V-doped devices, consistent with the barrier reduction between magnetic states[7]. Meanwhile, the RTN signals are suppressed at high doping concentrations (0.3 and 0.5% V) due to established stable ferromagnetic order (Supplementary Information Fig. 3). Temperature-dependent in-plane and out-of-plane MR hysteresis clearly indicate easy-axis in-plane anisotropic magnetic order (Extended Data Figs. 1, 2).

We next assess the reliability of the time evolution of resistance change and the corresponding RTN signal after ZFC and FC at V_{DC} = 0.85 V and T = 2 K (**Fig. 3a**). We defined the normalized resistance change $\Delta R_{norm}(\%) = [(R_H\text{-}R_L)/R_L]100$, R_H and R_L are resistance of high and low resistance states. The RTN signal is small with a negligible normalized jump (< 2%) but still persistent under ZFC. However, after FC at 0.1 T, $\Delta R_{norm,}$ increases to as large as ~5%. The histogram of the accumulated number of resistance changes clearly exhibits two discernable peaks These peaks become more predominant after FC at higher magnetic fields together with more discretized time intervals. With the FC at 5 T, a large value of ΔR_{norm} up to ~83% became apparent. We further measured RTN signals after FC with out-of-plane and in-plane magnetic fields of 1 T (Extended Data Fig. 3). The in-plane magnetization follows easy axis, leading to stronger magnetic fluctuations when applying an in-plane magnetic field during cooling process. The hard-axis out-of-plane RTN ΔR_{norm} is much larger by ~11% due to high activation barrier height than in easy-axis in-plane field RTN signal by ~2%.

We further analyze RTN signal based on the corresponding noise power spectrum density (PSD, $S_R(f)$) (**Fig. 3b** and Supplementary Information Fig. 4). The PSD under ZFC exhibited a flicker

noise ($S_R(f) \propto 1/f$, as shown in the left panel of **Figure 3b**, where f denotes the observed frequency. Meanwhile, the PSD under FC was well-fitted by the Lorentzian shape in the right panel, ($S_R(f) = S_0 \frac{1}{\left(1+\left(\frac{f}{f_C}\right)^2\right)} \propto 1/f^2$, where f_C denotes the cut-off frequency and S_0 represents the noise plateau of $S_R(f)$ for $f < f_C$. A $1/f^2$ feature with two discrete groups of energy levels under magnetic field was evidenced by two magnetic metastable states with a potential barrier. In our case, the time constant of high- and low-resistance levels can be extracted by collecting the number of data points in each duration time (right panel of **Fig. 3b**). For example, the analysis data for the RTN under FC of 0.1 T (the second panel of **Fig. 3a**) manifests the exponential relation between number of counts and duration time ($\propto \exp(-t/\tau)$, where τ denotes time constant for high or low state). The obtained average τ_{high} and τ_{low} are 1.69 s and 0.155 s with a cut-off frequency f_C (= $1/(2\pi\cdot\tau) = 1.12$ Hz, where $1/\tau = 1/\tau_{high} + 1/\tau_{low}$), which is consistent with f_C (= 1.27 Hz) determined from the PSD (**Fig.3b,** middle panel). We note that the extracted time constant of high- and low-resistance levels were well fitted to the exponential function regardless of temperature, bias, and ZFC/FC conditions (Supplementary Information Fig. 5). The determined cut-off frequency of the PSD under FC was reduced as the magnetic field increased (**Fig. 3c**). The activation energy E_a, $f_c = f_0 \exp(-E_a/k_BT)$, where k_B is the Boltzmann constant and T is temperature[2], was proportional to the magnetic field (*e.g.*, ΔE_a is ~3 meV as the magnetic field increases from 0.1 to 5 T), again confirming the presence of multiple magnetic states (Supplementary Information Fig. 4).

Such modulation of barrier energy after FC can be rationalized by a simple model for the formation of metastable magnetic states (**Fig. 3d**). After ZFC, the magnitude of noise with a single Gaussian histogram implies no discrete states, with equally probable E_a (**Fig. 3d**, top panel). After FC with different magnetic field (**Fig. 3d**, lower panel), the two discrete states emerge with a single

activation barrier (E_a'), which is confirmed by the presence of two-peak histograms. The activation barrier height is dependent on the magnetic field strength. The two discrete groups of energy states can be understood by the two magnetic states: parallel and antiparallel configurations of magnetic domains between V-doped WSe_2 magnetic layers, resembling the magnetic fluctuations in CoFeB/Mgo/CoFeB[7]. After FC with low magnetic field (*e.g.,* 0.01 T), the two magnetic states are not visible, with a small barrier height. In contrast, the activation barrier height is too high after FC with a high magnetic field of 10 T, which reduces the transition rate (Supplementary Information Fig. 6).

We further investigated the temperature-dependent time evolution of resistance changes and the corresponding RTN characteristics after FC process (**Fig. 4,** Extended Data Fig. 4, and Supplementary Information Figs. 7–9 for full data). Above 140 K (for example, at 180K), we observed a small ΔR_{norm} with a broad histogram. The Gaussian histogram of accumulated number of resistances reveals two peaks, one of which is slightly asymmetric, as supported by the deconvoluted curves (**Fig. 4a,** top panel). This strongly implies the fluctuation of multiple magnetic states together with persistent RTN from defects (*e.g.*, additional small resistance change below ~1%), in which we also observed in pure WSe_2 layers (Supplementary Information Fig. 2). This is again supported by the presence of two $1/f^2$ curves with two characteristic cut-off frequencies (**Fig. 4b**, top). At an intermediate temperature range of 70–140 K, additional giant RTN resistance changes appear (as high as ~30%) with two prevalent peaks, which are congruent with a single $1/f^2$ curve. These giant RTN changes are clearly measurable, well contrasted with the high-frequency RTNs that occur at high temperatures. Other giant RTN resistance changes (>40%) can be readily observed along with multiple other RTN changes at low temperatures (< 70 K), implying fluctuation of multiple magnetic states.

Since there are several ΔR_{norm}s due to the presence of multiple fluctuations of magnetic states, we collected all possible ΔR_{norm}s, where ΔR_{norm} is obtained from the two histogram peaks (**Fig. 4c**). We classified the resistance changes into three distinct categories in terms of $|\Delta R_{norm}|$ strength: small (~1%), intermediate (1% < $|\Delta R_{norm}|$ <10%), and giant (> 20%). We observed small $|\Delta R_{norm}|$ over the entire temperature range, which is typical for defective bulk materials[2]. Intermediate $|\Delta R_{norm}|$ also occur over a wide range of temperatures, in which we attributed to intralayer coupling due to magnetic domain-domain interaction between parallel and antiparallel alignments (**Fig. 4d**, top). Giant $|\Delta R_{norm}|$ appeared at temperatures below 140 K and became smaller due to thermal fluctuation of the spins, which were a consequence of interlayer magnetic coupling. The polarity of the ΔR_{norm} (**Fig. 4c**, inset) confirms the clear transition of magnetic fluctuations near ~70 K, which is in good agreement with the temperature-associated resistance change shown in **Figure 1b**. We note that the amplitudes of the noise power spectra for cut-off frequencies of f_{c2} resembles those observed for $|\Delta R_{norm}|$, although the magnetic transition was less clearly defined (**Fig. 4e**). This observation is analogous to the magnetic phase transitions seen in magnetic thin films[13]. It is worth mentioning that interlayer and intralayer magnetic interactions are also discernable in multilayer $CrBr_3$, although its phase transition temperature range is narrow from 21.4 -22.8 K[17]. In our V-doped WSe_2, we observed a wide range of transition temperatures, from 70–140 K.

Finally, we demonstrated functional magnetic devices in which we could tune inherent magnetic fluctuations by applying biases. The electric field and/or electrical current modulates the magnetic fluctuations of the junction device by varying biases (**Fig. 5a**). At low bias, the electric field prevails and introduces additional energy for metastable states through the magnetoelectric effect.[27] In contrast, current injection becomes dominant at high bias and hence induces spin-transfer torque between magnetic layers[34]. We first demonstrate a unique characteristic of

switching P and AP states using the bias. The RTN signals are measured at -0.8 V and 0.8 V after FC (out-of-plane magnetic field of 5 T) (**Fig. 5b**). The high resistance state appears at -0.8 V equivalent to antiparallel state, whereas the low resistance state emerges at 0.8 V equivalent to parallel state. This clearly features the switching between P and AP states with reversed biases. The remanent magnetization is generated during FC process formation of asymmetric states appears after FC, which may originate from the relative with respect to current flow in V-doped WSe_2. We note that this characteristic was not observed after ZFC due to their random remanent magnetization. Our device manifests a unique characteristic of switching P and AP states using bias, equivalent to combination of a unipolar RTN device CMOS circuit[7].

The dynamic range of resistances with varying biases is quite wide (**Fig. 5c**). Furthermore, I-V characteristics show the nonlinear behavior (Supplementary Information Fig. 10). Consequently, it shows rapid resistance change near nonlinear region (**Fig. 5c**). Therefore, designing peripheral circuitry that is able to adapt to the bias-dependent resistance ranges of each device could be a difficult task. In our case, the channel resistance was dropped by reducing the layer thickness. We fabricated another device (device 7) with thinner layers, d = 2 nm (Supplementary Information Fig. 11). The resistance was significantly dropped to ~k**Ω** range and more importantly, the resistance range was slowly modulated with varying biases (Extended Data Fig. 5). Despite small amplitudes of RTNs, we clearly modulate the number of jumps, which is suitable for device applications.

Furthermore, the speed of the RTN signals can be also modulated by biases. At a low bias of -0.7 V, the stochastic signals are negligible, with large resistance of a few G**Ω** due to insufficient current injection. Meanwhile, RTN fluctuations emerge at -0.75 V, with a small number of jumps with a slow cut-off frequency of 0.08 Hz (**Fig. 5c, d**). This indicates that the number of jumps increases

due to current injection. The number of jumps increases further to ~10 Hz as the bias rises, until the magnetic fluctuations become nearly stabilized at a high bias of -1.0 V due to spin-transfer torque (STT) saturation. We observed similar behavior in the positive polarity (Extended Data Fig. 6). We were also able to observe modulation of the number of jumps in another, identically designed device at 120 K (Extended Data Fig. 7). The time scale of our RTN device is slow in an order of milliseconds, still premature to reach high speed device. There is a tradeoff between cut-off frequency and amplitude of the RTN signal. For example, after FC at a reasonable magnetic field induces stable large RTN (Extended Data Fig. 8) whereas after FC at a high magnetic field, RTN signals were suppressed due to stabilized magnetic order (Supplementary Information Fig. 6). This suggests the magnitude of magnetic field cooling needs to be optimized with several other conditions. The time scale could be improved using several strategies such as V doping concentration, co-doping, surface functionalization, thickness, and gating.

So far, we clearly observed bistable magnetic states (*e.g.*, parallel (P) and antiparallel (AP) states) between low and high resistance states. To further rationalize the underlying mechanism of two resistance states in V-doped WSe_2 multilayer, we introduce spin-transfer torque via magnetic bilayers separated by nonmagnet layer (Supplementary Information Fig. 12a)[35]. The magnetization of free ferromagnetic layer (F2) can be switched parallel and antiparallel to the fixed ferromagnetic layer (F1). When electrons flow from F1 to F2, the spin momentum of the F1 will transfer to F2, switching the magnetization of F2 parallel to the magnetization of F1. In contrast, when electrons flow in opposite direction through F2, they reach F1 and reflect to F2. The reflected electrons contain the spin momentum opposite sign to that of F1, which can be switching magnetization of F2 antiparallel to the magnetization of F1. Consequently, the resistance can be switched between parallel configuration with small resistance to antiparallel configuration with large resistance. The

switching states in our vertical devices can be understood by a simple model of two STT devices with a common fixed magnetic layer (Supplementary Information Fig. 12b). In our device, there will be a charge transfer from graphene to p-doped V-WSe_2 layer to act as Schottky barrier[36]. The top V-doped WSe_2 layer is directly in contact with graphene layers, whereas the bottom V-doped WSe_2 layer is in contact with bottom graphene layers on SiO_2/Si substrate. This will yield asymmetric barrier height. The V-doped WSe_2 layers in our device are multilayered with typically ~5 nm or equivalently 5~7 layers. The spin magnetization in inner layers remain fixed, whereas the top and bottom surfaces are considered as free layers (or weak magnetization) and van der Waals gap is considered as a nonmagnet layer (Supplementary Information Fig. 12b). Similarly, the current direction can switch the magnetization of the top and bottom V-doped WSe_2 layers, *i.e.*, low resistance (parallel) and high resistance (antiparallel), as demonstrated in Fig. 5b with positive and negative bias.

We demonstrate another application to random number generator using RTN bitmap with time-dependent resistance changes of last panel in **Fig. 5c** (Extended Data Fig. 9). The time-evolution resistance data stream (4k bits = 2^{12}) measured at 2K after ZFC (Extended Data Fig. 9a) was arranged by 64 × 64 matrices to visualize high feasibility for random number generator (Extended Data Fig. 9b top panel). The absence of repeating patterns and blocks in Extended Data Fig. 9b clearly indicates high fidelity as a random number generator. Additionally, we digitized the bitmap image to clearly visualize high- and low-state of our RTN data stream (Extended Data Fig. 9b bottom panel). Since the insufficient number of data stream of our RTNs with unbalanced portion of high- and low-state, an ununiform distribution of white and black block can be seen in this figure. This limitation could be further tailored by electrical bias or operation temperature with a

long data acquisition time. To rationalize this approach clearly, the RTN stream data were numerically stacked by 10 times ($2^{12} \times 10$ = 40k bits, Extended Data Fig. 9c). Despite possible appearance of specific pattern driven by the stacking procedure, the generated bitmap image demonstrates the pseudo randomness without a noticeable pattern.

Conclusions

We have reported tunable magnetic fluctuations in heterostructured vdW magnetic semiconductor devices. The degree of magnetic order depends on several parameters including ZFC or FC at different magnetic fields, V-doping concentration, and temperature~~. For example, the bistable state is constructed at room temperature after ZFC at 0.1% V concentration, whereas the bistable state is diminished after FC (0.1 T) under the same conditions (Extended Data Fig. 10 and Supplementary Information Fig. 13)~~. For example, a bistable state is observed at room temperature after ZFC initialization for devices with a vanadium doping concentration of 0.1%, whereas the bistable state is diminished after FC (0.1 T) under the same conditions (Extended Data Fig. 10 and Supplementary Information Fig. 13). The RTN signal appears at low vanadium doping concentrations of 0.1%V and disappears at high vanadium doping concentration above 0.3% due to strong magnetic order. ~~Emergence of the RTN signals is directly correlated to magnetic domains as well. In our typical device, the lateral size was approximately ~10 x 5 μm^2. We checked the smaller sample size of 1 x 1 μm^2. The RTN signal was still maintained (Extended Data Fig. 10). Since the size of magnetic domains is in a nanometer scale for unstable magnetic states (*e.g.*, superparamagnetic[37]), we expect that the device size can be reduced to ~10 nm while the RTN signal is maintained. The detailed investigation is further required. The large RTN in signals associated with these magnetic fluctuations can be tuned by electrical biases. Our identification of a distinct transition of interlayer and intralayer magnetic order enriches the physics of magnetism~~

~~in 2D materials and opens the possibility of controlling magnetism in such systems based on the number of layers, stacking sequence, strain, and application of external biases. The fact that such tunable large resistance fluctuations can be obtained with a small activation energy could be important in low-power electronics.~~

The RTN signals is dependent on magnetic domains, and since the size of magnetic domains is on the nanometre scale for unstable magnetic states (such as superparamagnetic state[37]), we expect that the device size can be reduced down to around 10 nm without compromising the RTN signal. We measured RTN in devices with lateral dimensions of around 10 x 5 μm^2 and 1 x 1 μm^2 (Extended Data Fig. 10). The RTN signals associated with the magnetic fluctuations could be tuned using electrical biases, magnetic field, and temperature. We also identified transitions that correlate with the relative strength between interlayer and intralayer magnetic coupling strength, which could lead to the possibility of tuning the magnetic behaviour via the number of layers, stacking sequence, strain, and the application of external biases. Our observation of tunable resistance fluctuations with a small activation energy could be of use in the development of low-power electronics.

Methods

Single crystals of WSe_2 and V-doped WSe_2 were synthesized by the chemical vapor transport method with two steps. High-purity V (99.99%), W (99.999%), and Se (99.998%) powders (all from Sigma-Aldrich) were mixed at the desired concentration and pelletized, followed by annealing at 950 °C for 24 h. Iodine was then slowly added as a transport agent for the crystal growth step, as described in detail elsewhere[21]. The real V concentration ($V_xW_{1-x}Se_2$) revealing RTNs signal was 0.1%. The Gr/V-WSe_2/Gr vertical device was fabricated by the dry transfer

technique. The bottom graphene (Gr_{BT}) was directly exfoliated onto a SiO_2 substrate. Thickness of V-doped WSe_2 layer were measured by AFM 5000 II system (2~8 nm) (Supplementary Information Fig. 11), top graphene (Gr_T) flakes were exfoliated using polydimethylsiloxane (PDMS) and stacked onto the G_{BT} by the dry transfer method. The thickness of graphene layers is around 2~5 nm. The lateral size of devices is approximately 10x5 μm^2. The electrical characteristics of the heterostructures were assessed using a physical property measurement system (PPMS, Quantum Design) with an internal electrical transport option (ETO) module and an external Keithley 4200 system. Time-evolution RTN of resistance (R = V/I) was collected by applying the DC voltage (V) and measuring the current (I) using the Keithley 4200 with a current amplifier with a time interval of 1 ms. ZFC/FC R-T and magnetoresistance curves were obtained by applying AC voltage and measuring the AC current response with a current amplifier using the internal ETO mode of PPMS. The AC frequency is 0.1~0.5 Hz. The magnetic field is applied out-of-plane unless specified.

Data Availability

Code Availability (if relevant)

Acknowledgements This work was supported by the Institute for Basic Science (IBS-R011-D1) and Advanced Facility Center for Quantum Technology. P.K. acknowledge a partial support from ARO (W911NF-18-1-0366). M.-K.J. was supported by a NRF grant funded by the Korean government (MSIT) (NRF-2022R1A2C4001245) and by Sookmyung Women's University Research Grants (1-2203-2001).

Author Contributions Statement L.-A.T.N., J.J., and D.L.D. initiated this work. L.-A.T.N. fabricated and characterized devices. T.D.N. synthesized V-WSe_2 single crystals. M.-K.J.

performed noise analysis. D.L.D. and Y.H.L. guided the work. L.-A.T.N., P.K., M.-K.J., D.L.D., and Y.H.L. analyzed the data. All authors discussed and wrote the manuscript.

Competing Interests Statement: The authors declare no competing interests.

Tables

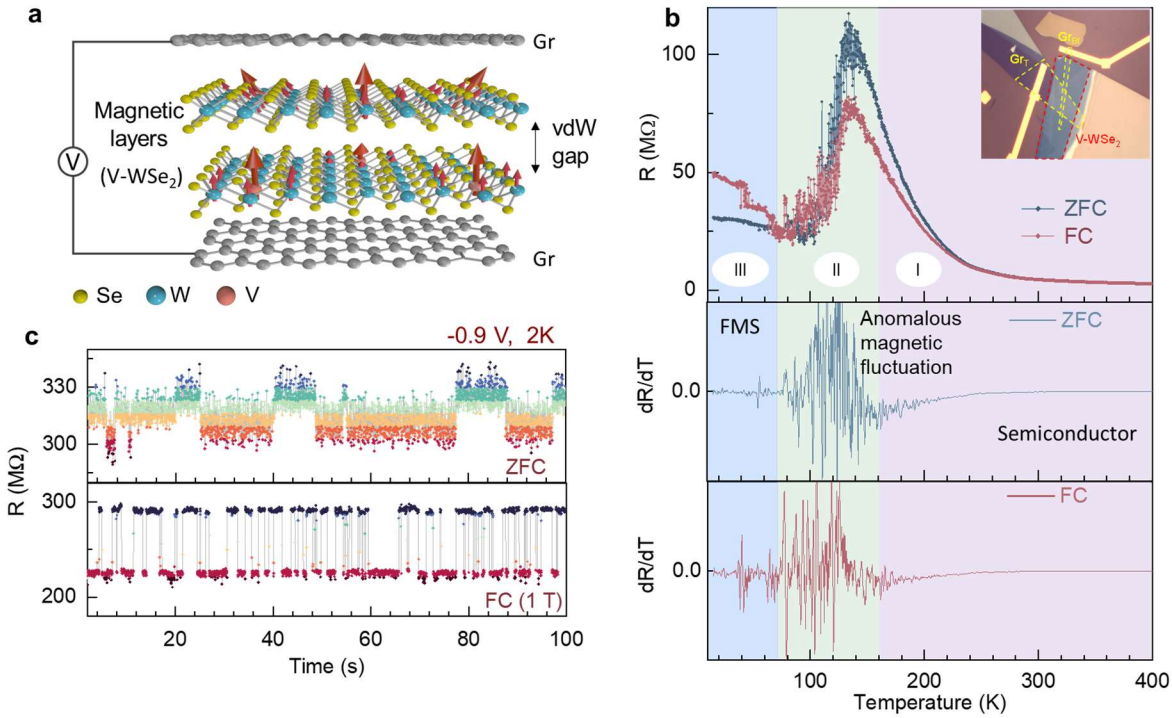


Figure 1 | Resistance changes with temperature and the identification of giant RTN in a vertical graphene/V-WSe_2/graphene device. a, Schematic of the device, with V-doped WSe_2 sandwiched between two graphene (Gr) layers, the red arrows represent the magnetic domains that can be generated around the vanadium atom. **b**, Temperature-dependent resistance R and its derivative dR/dT under zero-field cooling (ZFC) and field cooling (FC) with 1 T at V_{AC} = 0.9 V. Three distinct regions were identified: (I) semiconductor (light blue region), (II) anomalous magnetic fluctuation (green region), and (III) ferromagnetic semiconductor (purple region) with interlayer-coupled magnetic order. **c**, Time evolution of resistance change at 2 K, -0.9 V. The resistance mapping show characteristics of RTN with low resistance state (red) and high resistance state (dark blue) after ZFC (top panel) and FC (bottom panel). ~~a signature of RTN.~~ The data are measured in device 1 with 0.1% vanadium doping concentration.

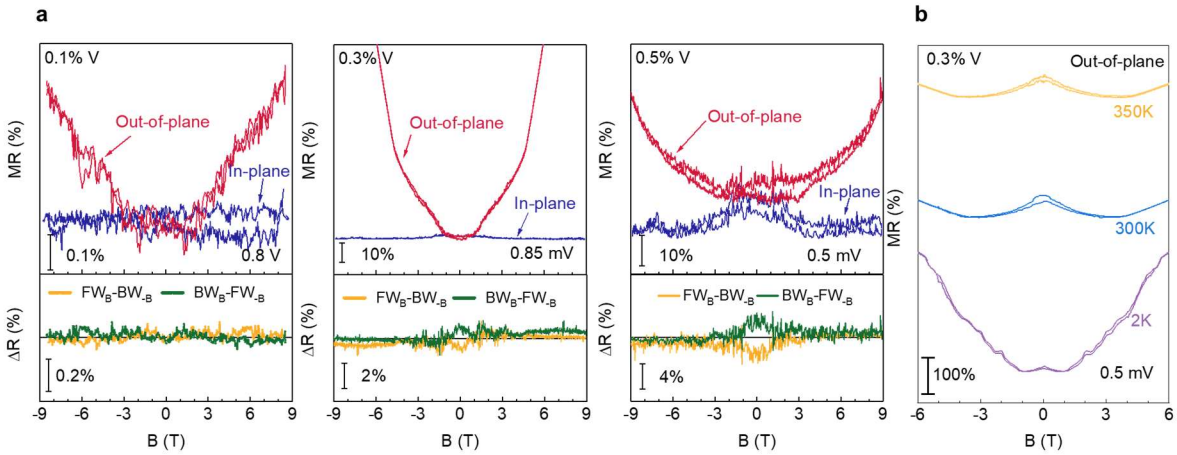
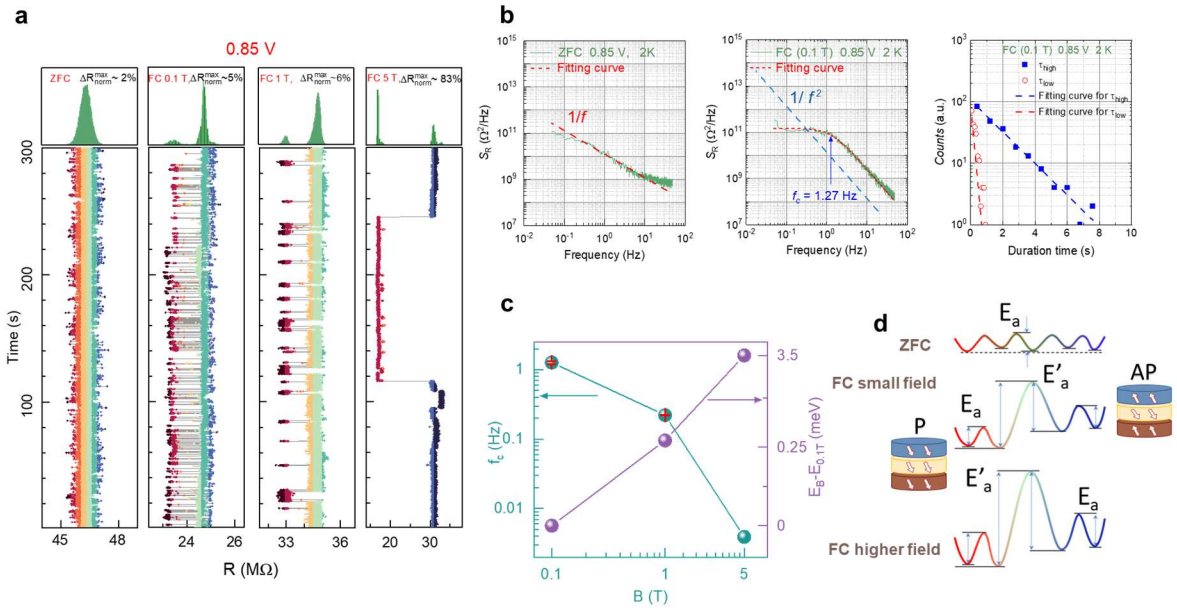


Figure 2 | MR hysteresis in V-doped WSe_2 at different V-doping concentrations. **a**, In-plane and out-of-plane magnetoresistance at 0.1% V, 0.3% V, and 0.5% V at 300 K. MR hysteresis is manifested at 0.3% and 0.5% V, confirming the stable ferromagnetic state. MR hysteresis is obscured in 0.1% V-doped WSe_2, indicating metastable magnetic states. All samples have similar thicknesses of ~ 2 nm. The biases of 0.8 V, 0.85 mV, and 0.5 mV are applied for corresponding 0.1%, 0.3%, and 0.5% V. **b**, Appearance of substantial hysteresis up to 350 K with a bias of 0.5 mV at 0.3% V, indicating the Curie temperature of higher than 350 K.



384

385 **Figure 3 | Control of RTN by magnetic fields. a**, RTN after ZFC and FC with magnetic fields of varying
386 strength (bottom) and the corresponding histograms (top). The resistance mapping show characteristics of
387 RTN with low resistance state (red) and high resistance state (dark blue). Data are collected at 2 K, 0.85 V.
388 **b**, Analysis of RTN signal after ZFC and FC (0.1 T) and the corresponding time constants of high and low
389 resistance levels. **c**, Cut-off frequency (f_c) of $1/f^2$ noise and extracted energy barrier changes after FC
390 processes with magnetic fields of varying strength. **d**, Schematic of the multiple metastable states from low
391 resistance state (red) to high resistance state (dark blue) with equally probable activation energy Ea after
392 ZFC (top panel), and after FC with different magnetic field (lower panels) the two discrete states are parallel
393 (P) and antiparallel (AP) emerge with a single activation barrier (E_a'). The data are measured in device 1
394 with 0.1% vanadium doping concentration.

395

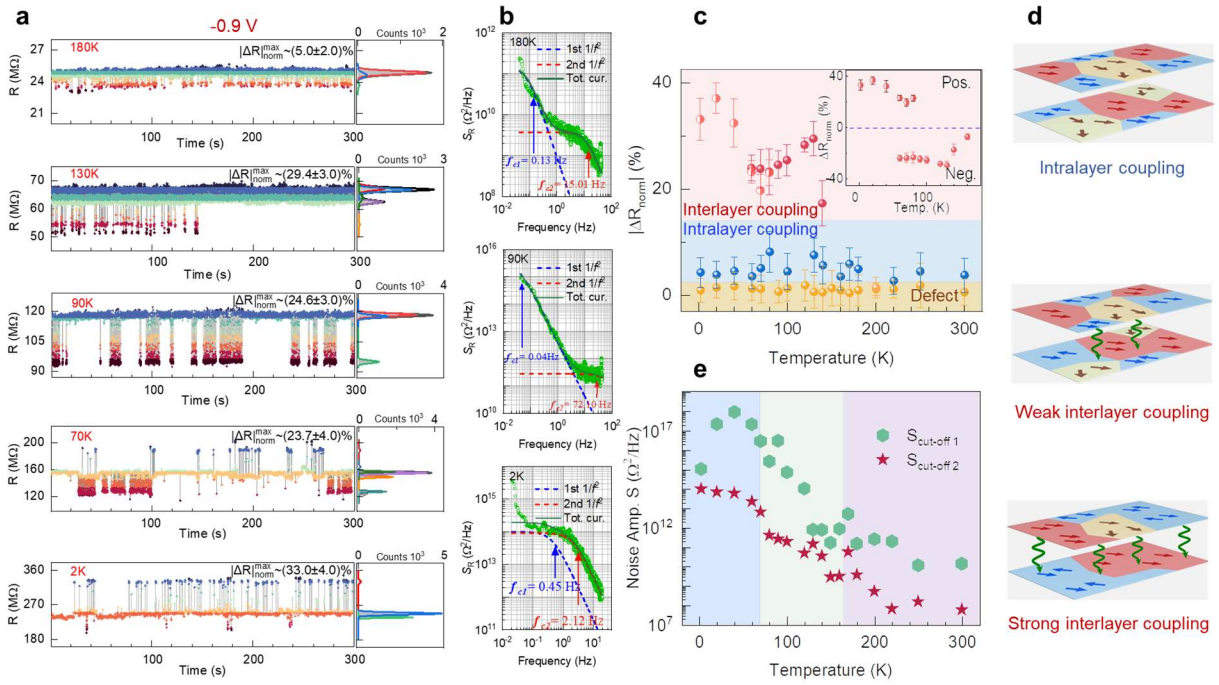
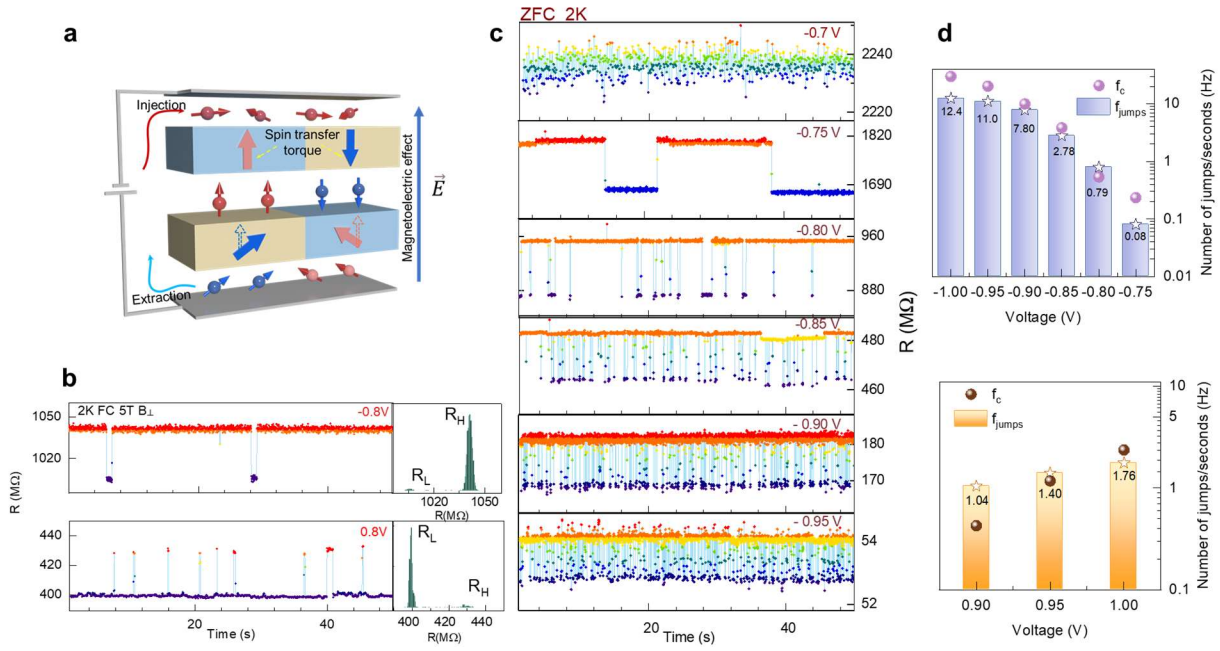


Figure 4 | Temperature-dependent RTN across the vertical Gr/V-WSe_2/Gr junction after FC. a, RTN at five different temperatures in three different regions at -0.9 V. RTN at 2, 90, and 180 K respectively correspond to regions I, II, and III in **Figure 1b**. RTN at 70 and 130 K corresponds to boundaries of region I-II and II-III, respectively. Histograms are shown at right with deconvoluted curves (different color curves: blue, green, red …) presence of multiple fluctuations of magnetic states. **b,** Noise spectra representing three different zones with multiple $1/f^2$ curves; intralayer coupling at high temperature (top panel), weak interlayer coupling at intermediate temperature (middle), and strong interlayer coupling at low temperature (bottom). **c**, Evolution of $|\Delta R_{\mathrm{norm}}|$ (dot symbols) at different temperatures. The resistance changes into three distinct categories in terms of $|\Delta R_{\mathrm{norm}}|$ strength: small (yellow), intermediate (blue), and giant (red) correspond defect, intralayer coupling and interlayer coupling regions. Inset is the polarity change of ΔR_{norm}. Obvious distinguishing regions are revealed. **d**, Schematic of three different interactions with magnetic domains: i) intralayer coupling, ii) weak interlayer coupling, iii) strong interlayer coupling. **e**, Temperature-dependent noise amplitude at two cut-off frequencies f_{c1} (blue) and f_{c2} (red) corresponding three distinct regions were identified: (I) semiconductor (light blue region), (II) anomalous magnetic fluctuation (green region), and (III) ferromagnetic semiconductor (purple region) with interlayer-coupled magnetic order. The data were measured in device 1 with 0.1% vanadium doping concentration



414

415 **Figure 5 | Control of RTNs across the vertical Gr/V-WSe_2/Gr junction by biases after ZFC process.**
416 **a,** Schematic of energy introduced to the magnetic metastable phases by electric fields. **b**, RTN signal after
417 FC (5 T) at 2 K demonstrates the switching between P and AP states with reversed biases (+0.8 and -0.8
418 V). **c**, RTN as measured over a range of biases. The data are collected at 2 K after ZFC process. **d,** Frequency
419 of jumps f_{jumps} (start) are calculated by number of jumps per seconds and cut-off frequency fc (dot) in the
420 device at different biases. The data are measured in device 2 (see Supplemental Table 1) with 0.1% of
421 vanadium doping concentration.
422

References

1. Jevtić, M. M. Noise as a diagnostic and prediction tool in reliability physics. *Microelectronics Reliability* **35**, 455–477 (1995).

2. Grasser, T. *Noise in Nanoscale Semiconductor Devices*. *Noise in Nanoscale Semiconductor Devices* (Springer International Publishing, 2020). doi:10.1007/978-3-030-37500-3.

3. Grollier, J. *et al.* Neuromorphic spintronics. *Nature Electronics* **3**, 360–370 (2020).

4. Marković, D., Mizrahi, A., Querlioz, D. & Grollier, J. Physics for neuromorphic computing. *Nature Reviews Physics* **2**, 499–510 (2020).

5. Camsari, K. Y., Faria, R., Sutton, B. M. & Datta, S. Stochastic p-bits for invertible logic. *Physical Review X* **7**, 1–19 (2017).

6. Camsari, K. Y., Sutton, B. M. & Datta, S. P-bits for probabilistic spin logic. *Applied Physics Reviews* **6**, (2019).

7. Borders, W. A. *et al.* Integer factorization using stochastic magnetic tunnel junctions. *Nature* **573**, 390–393 (2019).

8. Hayakawa, K. *et al.* Nanosecond Random Telegraph Noise in In-Plane Magnetic Tunnel Junctions. *Physical Review Letters* **126**, 117202 (2021).

9. Safranski, C. *et al.* Demonstration of Nanosecond Operation in Stochastic Magnetic Tunnel Junctions. *Nano Letters* **21**, 2040–2045 (2021).

10. Ghosh, S., Kargar, F., Mohammadzadeh, A., Rumyantsev, S. & Balandin, A. A. Low-Frequency Electronic Noise in Quasi-2D van der Waals Antiferromagnetic Semiconductor FePS 3 — Signatures of Phase Transitions. *Advanced Electronic Materials* **7**, 2100408 (2021).

11. Kundu, H. K. *et al.* Quantum Phase Transition in Few-Layer NbSe2 Probed through Quantized

Conductance Fluctuations. *Physical Review Letters* **119**, 1–6 (2017).

12. Valle, J. del *et al.* Generation of Tunable Stochastic Sequences Using the Insulator–Metal Transition. *Nano Letters* acs.nanolett.1c04404 (2022) doi:10.1021/acs.nanolett.1c04404.

13. Weissman, M. B. & Israeloff, N. E. Electrical noise measurements on magnetic films (invited). *Journal of Applied Physics* **67**, 4884–4888 (1990).

14. Raquet, B., Anane, A., Wirth, S., Xiong, P. & Von Molnár, S. Noise probe of the dynamic phase separation in La2/3Ca1/3MnO3. *Physical Review Letters* **84**, 4485–4488 (2000).

15. COLLINS, M. F. *Magnetic critical scattering*. (OXFORD UNIVERSITY PRESS, 1989).

16. Mermin, N. D. & Wagner, H. Absence of ferromagnetism or antiferromagnetism in one- or two-dimensional isotropic Heisenberg models. *Physical Review Letters* **17**, 1133–1136 (1966).

17. Jin, C. *et al.* Imaging and control of critical fluctuations in two-dimensional magnets. *Nature Materials* **19**, 1290–1294 (2020).

18. Nair, G. K. R. *et al.* Phase-pure two-dimensional FexGeTe2 magnets with near-room-temperature TC. *Nano Research* **15**, 457–464 (2022).

19. Yun, S. J. *et al.* Ferromagnetic Order at Room Temperature in Monolayer WSe2 Semiconductor via Vanadium Dopant. *Advanced Science* **7**, 1–6 (2020).

20. Song, B. *et al.* Evidence of itinerant holes for long-range magnetic order in tungsten diselenide semiconductor with vanadium dopants. *Physical Review B* **103**, (2020).

21. Jiang, J. *et al.* Probing giant Zeeman shift in vanadium-doped W Se 2 via resonant magnetotunneling transport . *Physical Review B* **103**, 1–9 (2021).

22. Merithew, R. D. *et al.* Mesoscopic thermodynamics of an inhomogeneous colossal-magnetoresistive phase. *Physical Review Letters* **84**, 3442–3445 (2000).

23. Zhu, M., Li, X., Xiang, G. & Samarth, N. Random telegraph noise from magnetic nanoclusters in the ferromagnetic semiconductor (Ga,Mn)As. *Physical Review B - Condensed Matter and Materials Physics* **76**, 10–13 (2007).

24. Klein, D. R. *et al.* Probing magnetism in 2D van der Waals crystalline insulators via electron tunneling. *Science* **3617**, 1–9 (2018).

25. Song, T. *et al.* Giant tunneling magnetoresistance in spin-filter van der Waals heterostructures. *Science* **360**, 1214–1218 (2018).

26. Huang, B. *et al.* Electrical control of 2D magnetism in bilayer CrI 3. *Nature Nanotechnology* **13**, 544–548 (2018).

27. Jiang, S., Shan, J. & Mak, K. F. Electric-field switching of two-dimensional van der Waals magnets. *Nature Materials* **17**, 406–410 (2018).

28. Baibich, M. N. *et al.* Giant magnetoresistance of (001)Fe/(001)Cr magnetic superlattices. *Physical Review Letters* **61**, 2472–2475 (1988).

29. Yuasa, S., Nagahama, T., Fukushima, A., Suzuki, Y. & Ando, K. Giant room-temperature magnetoresistance in single-crystal Fe/MgO/Fe magnetic tunnel junctions. *Nature Materials* **3**, 868–871 (2004).

30. Parkin, S. S. P. *et al.* Giant tunnelling magnetoresistance at room temperature with MgO (100) tunnel barriers. *Nature Materials* **3**, 862–867 (2004).

31. Telford, E. J. *et al.* Coupling between magnetic order and charge transport in a two-dimensional magnetic semiconductor. *Nature Materials* **21**, 754–760 (2022).

32. Ohta, T. *et al.* Butterfly-shaped magnetoresistance in van der Waals ferromagnet Fe 5 GeTe 2. *AIP Advances* **11**, 025014 (2021).

33. Zhuo, W. *et al.* Manipulating Ferromagnetism in Few-Layered Cr 2 Ge 2 Te 6. *Advanced Materials* **33**, 2008586 (2021).

34. Cao, W., Wei-Yuan Tu, M., Xiao, J. & Yao, W. Giant Spin Transfer Torque in Atomically Thin Magnetic Bilayers. *Chinese Physics Letters* **37**, (2020).

35. Coey, J. M. D. *Magnetism and Magnetic Materials*. *Nucl. Phys.* vol. 13 (Cambridge University Press, 2001).

36. Song, B. *et al.* Evidence of itinerant holes for long-range magnetic order in the tungsten diselenide semiconductor with vanadium dopants. *Physical Review B* **103**, (2021).

37. Li, Q. *et al.* Correlation between particle size/domain structure and magnetic properties of highly crystalline Fe3O4 nanoparticles. *Scientific Reports* **7**, 9894 (2017).

Supplementary information is linked to the online version of the paper at www.nature.com/nature.

Author information Reprints and permissions information is available at www.nature.com/reprints. The authors declare no competing financial interests. Readers are welcome to comment on the online version of this letter at www.nature.com/nature. Correspondence and requests for materials should be addressed to M.-K.J. (mkjoo@sookmyung.ac.kr), D.L.D. (l.duong1902@gmail.com), Y.H.L. (leeyoung@skku.edu).

508

509